Characterization of single channel liquid light guide coupling and SPAD array imaging for tumour margin estimation using fluorescence lifetime

OPEN ACCESS
IOP Publishing
Measurement Science and Technology
Meas. Sci. Technol. **31** (2020) 125701 (12pp)
https://doi.org/10.1088/1361-6501/aba5c6

Characterization of single channel liquid light guide coupling and SPAD array imaging for tumour margin estimation using fluorescence lifetime

Hazel L Stewart[1], **Graham Hungerford**[2] and **David J S Birch**[1,2]

[1] Department of Physics, The Photophysics Research Group, Centre for Molecular Nanometrology, University of Strathclyde, SUPA, John Anderson Building, 107 Rottenrow East, Glasgow G4 0NG, United Kingdom
[2] HORIBA Jobin Yvon IBH Ltd., 133 Finnieston Street, Glasgow G3 8HB, United Kingdom

E-mail: djs.birch@strath.ac.uk

Received 28 February 2020, revised 4 July 2020
Accepted for publication 14 July 2020
Published 30 September 2020

Abstract

Surgery remains one of the key treatment options for tumour removal, and surgeons primarily rely on eye and touch to assess the boundary between healthy and cancerous tissue with no cellular information as guidance. There is therefore a need for a device or instrument that can be used by the surgeon in real-time during the surgical procedure to ensure as many of the cancerous cells and as few of the healthy cells have been removed as possible. Fluorescence approaches have previously demonstrated significant promise in this application, but clinical take-up has been limited and much more characterization of critical parameters needed before robotic surgery can be contemplated. Here we investigate two time-correlated single-photon counting (TCSPC) fluorescence lifetime systems for the detection of phantom tumour margins derived from silica sol-gels. A simple and low-cost liquid light guide system (LLG) incorporating a single photomultiplier detection channel and translational stage was developed. This provided a useful reference for a compact single-photon avalanche diode (SPAD) array camera system for fluorescence lifetime imaging microscopy (FLIM) which permits up to ~25 000 in-pixel timing measurements at video rates in ambient light using only low energy (~30 pJ) diode laser pulses to minimize cell and dye degradation. Measurements of phantom margins with sol-gel doped Rhodamine 6G (R6G) of fluorescence lifetime ~4 ns using the LLG system demonstrates that for 7 mm excitation diameter and over 5–15 mm sol-gel LLG separation the sol-gel only region could be clearly identified 1 mm after the margin position, a widely accepted minimum surgical resolution. A comparison between measurements with the LLG and SPAD FLIM system using the sub-ns fluorescence lifetime of the FDA-approved dye indocyanine green (ICG) demonstrates that the minimum workable spatial resolution and sufficient speed are only achievable with such faster lifetimes using the SPAD FLIM system.

Supplementary material for this article is available online

Keywords: fluorescence lifetime, FLIM, silica sol-gel, tissue phantom, tumour margin estimation, indocyanine green

(Some figures may appear in colour only in the online journal)

1. Introduction

Cancer is one of the leading causes of death worldwide, with over 18 million cases diagnosed globally in 2018 [1]. This is set to rise to over 29 million diagnoses by 2040 [1], and so the continuous development and improvement of cancer treatment remains of high importance. There are several treatment options available to cancer patients, which are typically chosen depending on the type and stage of cancer such as chemotherapy, radiation therapy and surgery. While many cancer treatments are currently being developed, surgery remains one of the most common treatment options for tumour removal and in the UK ~49% of all patients cured undergo surgical intervention [2].

During cancer surgery it is important that as much of the cancerous tissue is removed as possible while also preventing unnecessary damage to surrounding healthy tissue [3]. To accomplish this surgeons primarily rely on visual inspection, palpation and previous experience in order to determine the cancerous tissue. While this can be effective for bulk tumour it lacks sensitivity in detecting cancer at the cellular level [4], potentially leading to the patient requiring further surgery if cancerous cells remain in the body. The margin between the cancerous cells and the cut tissue edge is known as the surgical margin, where the current gold standard for margin assessment is slide-based histology. This however has to be completed post-operatively, and is often a time-consuming and laborious process [5]. There are certain techniques currently available for estimating tumour margins intraoperatively, some of which include frozen section histology, intraoperative MRI, CT [6], ultrasound [7] and optical coherence tomography [8]. However these have their own drawbacks and are not in widespread use, where some drawbacks include requiring highly complex and specialized surgical suites for the use of intraoperative MRI and CT in particular, which are also currently limited in their use to neurosurgery [6], as well as other techniques being limited in spatial resolution and contrast compared to post-operative histology [5]. New technologies for intraoperative margin assessment need to be able to match the diagnostic accuracy of post-operative histology and bring further benefits such as reduced turnover times, practicality and reduced cost before they can be considered for routine clinical practice [9].

One area that has gained significant interest for intraoperative margin assessment in recent years is the use of fluorescence-based techniques. Such techniques have many advantages for their use in margin estimation which include high contrast and sensitivity, intuitive operation, relatively low cost, ease of image acquisition as well as high selectivity for certain cancer cells [6, 10]. Two of the main oncological applications for fluorescence include sentinel lymph node (SLN) mapping where a fluorescent dye can be used to visualize the location of the SLN using a low dose of contrast agent [6], as well as in tumour imaging for visualizing cancerous tissue, where fluorescent agents have the ability to detect small tumour lesions that could be easily missed during surgery. Recent developments in tumour imaging using fluorescence-based techniques include the use of fluorescence lifetime imaging microscopy (FLIM) for visualizing autofluorescence from components such as the reduced form of the coenzyme nicotinamide adenine dinucleotide and its phosphorylated derivative (NAD(P)H) and flavin adenine dinucleotide (FAD) in various tissues and cell studies to distinguish between healthy and cancerous regions [11–13]. The development of new extrinsic probes is also of interest, where one example is the use of an antibody conjugated to a near infrared (NIR) dye for determining squamous cell carcinomas in the head and neck [14].

Developments in complementary instrumentation are also taking place. Indeed a range of commercially available steady-state fluorescence systems intended for surgical applications are already starting to appear, for example the PerkinElmer IVIS® Spectrum [15, 16] and the FLUOBEAM® camera system [17]. However, being steady-state such systems are prone to analogue fluctuations such as photochemical bleaching of the sensor fluorophore, cell phototoxicity and fluorescence collection variations when studying structured surfaces such as tissue. The digital nature of time-correlated single photon counting (TCSPC) fluorescence lifetime measurements applied to imaging automatically generates images that are free from analogue fluctuations in fluorescence intensity. In this regard recent improvements in single-photon avalanche diode (SPAD) arrays for real-time FLIM [18] in terms of array size, sensitivity, robustness when operating in ambient light at workable visual levels, successful operation with compact and low power diode sources (mW) to minimize cell and dye degradation, high sensitivity in the near infra-red, video rate data acquisition and user-friendly software combine to offer realistic possibilities in surgery. A SPAD array-based fluorescence sensor has indeed previously been shown to distinguish subtle lifetime differences in healthy and cancerous tissue in mouse models [19], however quantification of the surgical margin as we report here has yet to be fully explored.

While many instruments and methods are currently being researched and developed, most are still in pre-clinical stages, use steady-state fluorescence and are limited to specific FDA-approved fluorophores. The ability to operate in an ambient light setting is not hitherto fully realised [20], and only being

able to image macroscopically, although adequate for incision, does not yield the complementary *in vivo* microscopic cellular information [21] that critically supports margin estimation. The consequence of these limitations is that surgeons still largely rely on vision and touch. Continued research, development and characterization of these techniques is required to try and eliminate the drawbacks and further advance the field of margin estimation, finding a cost-effective and practical solution for surgeons to use in accurately identifying margins intraoperatively.

In this work we present two fluorescence-based methods for the detection of phantom tumour margins derived from silica sol-gels. A TCSPC fluorescence lifetime spectroscopy system has first been adapted to operate 'out-of-the-box' by incorporating liquid light guides (LLGs) and a translational stage in order to measure across a phantom tumour margin, where the fluorophores Rhodamine 6G (R6G) and FDA-approved indocyanine green (ICG) were added to the silica sol-gel to create the phantom margin. Although single-mode optical fibres and their bundles have been widely used in endoscopy, the use of LLGs has been little investigated despite their higher throughput for conveying optical signals and better intrinsic robustness for everyday use. This low-cost LLG system provides an important reference on the same samples when compared to FLIM measurements performed on a prototype HORIBA IBH FLIMera fluorescence lifetime imaging camera based on the QuantiCam SPAD camera [22] and HORIBA IBH *Eztime Image* software. The latter brings key advantages to bear in a single system. These include the ability to operate at sufficient ambient light levels compatible with visual inspection, imaging down to cellular levels when combined with wide-field microscope optics [22], video rate imaging and independence of analogue fluctuations.

Measurements of the phantom margin with R6G in the doped sol-gel region demonstrated the sol-gel only region could be clearly identified 1 mm after the margin position based on the fluorescence decays obtained using the LLG-based system. Improved spatial resolution was demonstrated with the FLIM system for measurements of the ICG phantom margin. Measurements of ICG on the LLG-based system demonstrated that only scatter from the dye region of the sol-gel could be detected 7 mm before the margin was reached for an excitation spot ~7 mm in diameter, whereas FLIM images could be obtained in almost real-time to much more accurately identify the sol-gel only region 1 mm after the margin position. Having methods that can rapidly determine surgical margins to millimetre precision would be extremely beneficial in cancer surgery, where fluorescence lifetime spectroscopy has been shown here to be capable of such precision from real-time measurements that take <2 min to traverse the margin. The complete image capability of SPAD-based photon timing cameras opens up new capabilities for tumour margin estimation as described here, that were not hitherto possible by multiplexing a discrete number of detection channels [23]. Results obtained with both systems not only serve to define some of the measurement parameters and boundaries that are useful in their specific implementations, but also might inform integration of such technologies into more automated surgical systems when assessing the feasibility of some of the longer-term goals with robotic surgery.

2. Methods and materials

2.1. Fluorescence lifetime spectroscopy instrumentation

Fluorescence decay measurements were performed using TCSPC on an adapted HORIBA IBH TemPro system. The system was initially adapted to incorporate two 1 m LLGs (Newport) that had a transmittance range of 340–800 nm, a core diameter of 3 mm, and a numerical aperture of 0.59 resulting in an acceptance cone of 72°. The LLG design is much like that of a single silica fibre but with a larger core diameter in comparison, where the core consists of a sealed liquid to carry the light instead of a conventional glass core. LLGs have been little if at all explored in surgical margin applications and yet they offer a number of advantages when compared to conventional silica fibre-based bundles that are more often reported. One is that there is the ability to transmit more light due to the open cross-section where all the space can be used to transmit light with total reflectance. Fibre bundles instead consist of multiples of fibres where light is lost in the space between the individual fibres. LLGs are also more flexible due to the polymer tubing used compared to silica fibres which are prone to breakage when frequently bent, making light guides potentially more suitable for certain surgical applications due to their robustness. In addition to these factors LLGs often have a higher numerical aperture than silica fibre bundles, where the larger acceptance angle allows for the collection of more light. Of course theoretically the smaller the light-guide diameter the better the resolution, but the trade-off is unworkably low fluorescence collection and concomitant increased susceptibility to surface contamination. Hence we adopted a different route to determine what spatial resolution was achievable with LLGs and if it was simply a function of LLG diameter. A translational stage (ThorLabs) was also incorporated as the sample stage and a holder for the LLGs was designed to keep the light guides at a fixed position and distance above the sample. A schematic of the setup is shown in figure 1, illustrating how the LLGs were utilized for the measurement of fluorescence lifetimes as a means of transmitting the signal from the excitation source as well as collecting fluorescence from the sample.

Holders were designed for coupling HORIBA IBH NanoLED excitation sources [24] and TBX detectors to the LLGs, where each of the couplings had space for neutral density or longpass filters for emission wavelength selection as required. Each coupling was also designed to be as light tight as possible to minimize the collection of background light. The LLG guide carrying excitation light is perpendicular to the sample, whereas the LLG carrying fluorescence to the detector is fixed at 45° to minimize excitation light being collected by this light guide. This minimizes the surface scatter problems frequently encountered when using a single bifurcated light guide and

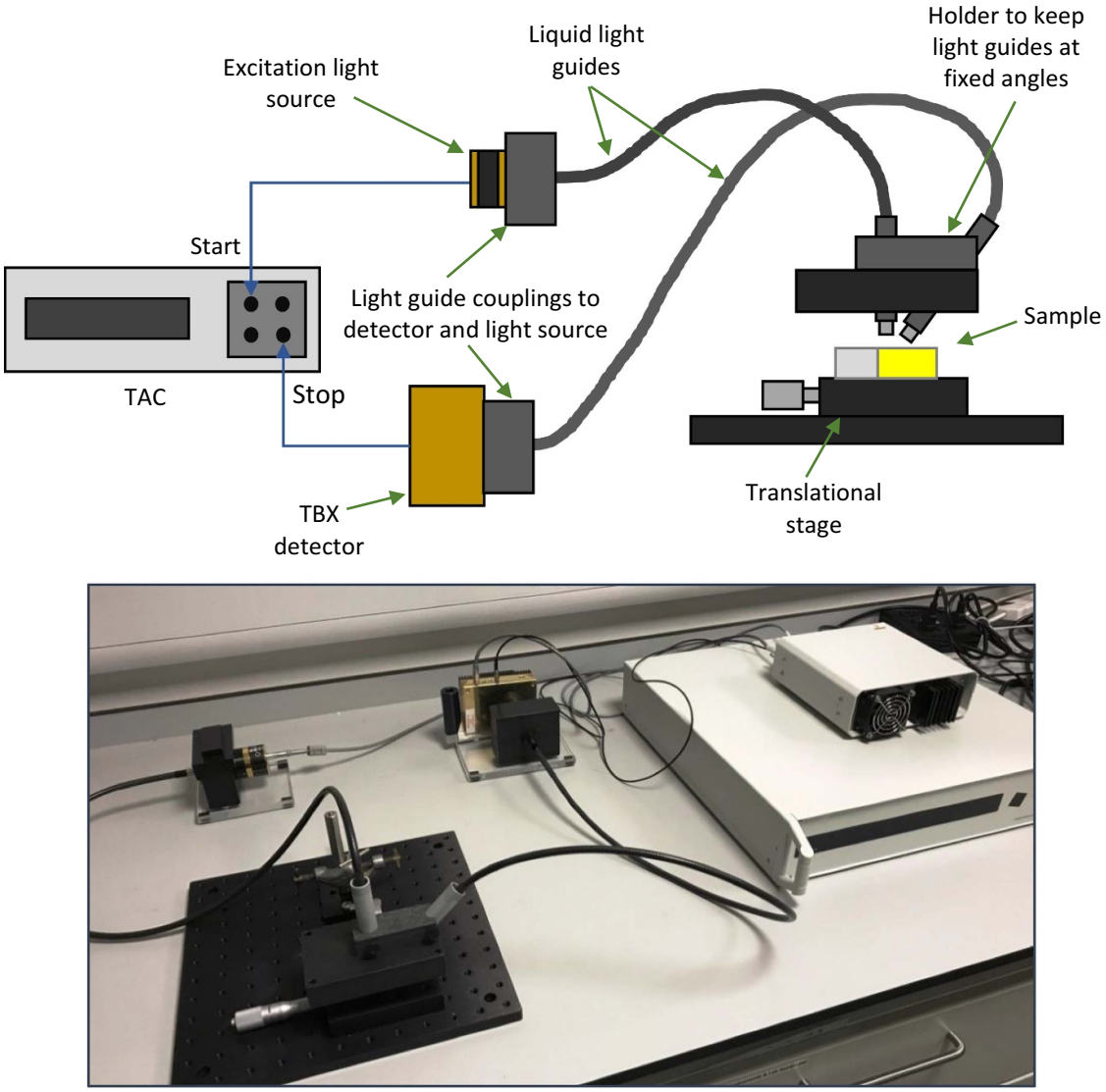

Figure 1. Schematic of the adapted TCSPC fluorometer incorporating liquid light guides and a translational stage for the fluorescence decay measurement of phantom tumour margins, along with a photograph of the setup.

Table 1. Fluorescence lifetime parameters and normalized χ^2 goodness of fit obtained from reconvolution analysis of equation (1) from measurements of CG436 and R6G in water on a HORIBA IBH DeltaFlex fluorescence lifetime system that incorporates a Seya-Namioka monochromator on the emission arm for emission wavelength selection (Mono.) and the translational stage-based liquid light guide system shown in figure 1.

Sample	λ_{ex} (nm)	λ_{em} (nm)	System Setup	τ_1 (ns)	f_1 (%)	τ_2 (ns)	f_2 (%)	τ_{avg} (ns)	χ^2
CG436	339	440	Mono.	18.4 ± 1.1	56.95	26.9 ± 0.6	43.05	21.3	1.12
			LLG	16.0 ± 1.0	46.49	27.9 ± 0.4	53.51	20.7	1.18
R6G	474	560	Mono.	4.06 ± 0.01	100	-	-	4.06	1.19
			LLG	3.99 ± 0.01	100	-	-	3.99	1.03

was chosen vs the reverse excitation-fluorescence configuration in order to provide a more realistic tissue simulation by maximizing the excitation light penetration depth in the phantom. The sample stage could be moved left to right in one plane over a 25 mm distance to measure different positions of a sample. The LLG holder could be moved up and down as required, and in addition to this the position of the light guides themselves in the holders could be moved. Fluorescence lifetime measurements using this setup were typically performed with the light guides at a height of 5 mm from the sample surface giving an excitation spot of ~7 mm diameter. Measurements were performed in a dark room with a black cloth also placed over the setup to further minimize ambient light detection.

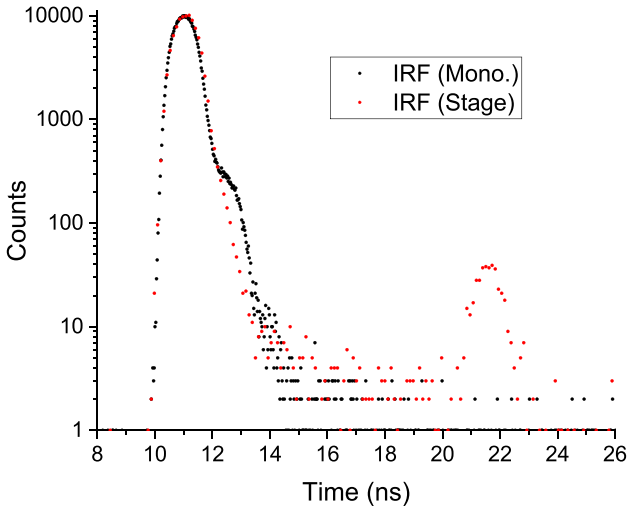

Figure 2. Instrumental response functions (IRF) obtained from a dilute LUDOX SM-AS scattering sample and 339 nm excitation on the monochromator-based DeltaFlex system (Mono) and the liquid light guide and translational stage-based system (LLG/stage) and used in the CG436 reconvolution measurements shown in table 1. The full width at half maximum (FWHM) of the IRF for the Mono and LLG/stage systems were 0.98 ns and 1.10 ns, respectively, and the FW(1%)M of the IRFs were 2.88 ns and 2.52 ns, respectively. The smaller peak at ~10 ns after the main peak in the stage measurement is due to reflection from the end of the light guide.

To initially assess the suitability of the LLG-based system, the fluorescence decays of several fluorophores were measured with varying excitation, emission and lifetime properties. The results for two of these fluorophores are shown in table 1, which include CG436 (6-methoxy-1-methyl quinolinium bromide) and R6G. The fluorescence lifetime properties of the fluorophores chosen are well documented in literature [25, 26]. Excitation sources with wavelengths λ_{ex} of 339 nm (CG436) and 494 nm (R6G) were used alongside emission wavelengths λ_{em} of 440 nm and 560 nm, respectively. For comparison, the fluorescence decays of each fluorophore were measured on the LLG-based system as well as on a conventional HORIBA IBH DeltaFlex system incorporating an f/3 Seya-Namioka geometry emission monochromator (Mono.). This geometry minimizes stray light rejection and temporal dispersion (0.13 ps nm^{-1}) by virtue of its minimal number of optical components comprising a concave holographic grating and only two mirrors. As well as varying in excitation and emission wavelength, these fluorophores also varied in fluorescence lifetime, ranging from the shorter lifetime of R6G (τ_{avg} ~ 4 ns) to that of CG436 (τ_{avg} ~ 21 ns). A comparison of the results in table 1 shows that the lifetime parameters obtained for each of the fluorophores are in good agreement with values reported previously [25, 26] on both lifetime systems. This demonstrates that the LLG-based system is capable of obtaining reliable fluorescence lifetime data over a range of wavelengths and timescales. A comparison of the instrumental response functions (IRFs) on each system (obtained by detecting scattered excitation from a dilute LUDOX SM-AS colloidal silica sample) are also shown in figure 2 and are consistent, implying comparable limits in lifetime resolution for both systems.

For measurements of R6G in the phantom margin, a 474 nm NanoLED pulsed diode laser excitation source (~7 pJ per pulse at 1 MHz repetition rate) and a 560 nm Schott glass longpass filter for emission wavelength selection were used. Excitation of ICG could also be achieved at low pulse energies using a 775 nm HORIBA IBH pulsed DeltaDiode laser excitation (~30 pJ per pulse at 100 MHz repetition rate) [27], and an 800 nm longpass filter was used for emission wavelength selection. Further diode wavelengths and optical filters are available for commonly used dyes for both the LLG and FLIM systems.

2.2. FLIM instrumentation

FLIM measurements were performed using a prototype HORIBA FLIMera SPAD camera, where a photograph of this system is shown in figure 3. The setup utilized DeltaDiode pulsed laser diode sources for excitation of samples, allowing for repetition rates of up to 100 MHz. Excitation light is directed to the sample via a dichroic mirror, where fluorescence is transmitted through the mirror and a longpass filter for emission wavelength selection before reaching the FLIMera camera incorporating a QuantiCam SPAD-TDC array. The QuantiCam is based on STMicroelectronics 40 nm CMOS technology fabricated into 192 × 128 SPAD pixels of dimensions 18.4 μm × 9.2 μm with a 13% fill factor [22]. Each individual pixel incorporates its own TCSPC electronics-based time-to-digital converter (TDC). This enables the rapid collection of fluorescence lifetime data in every one of the 24 576 pixels simultaneously, which are then fed into the *EzTime Image* PC software for collection and data analysis.

For measurements of the ICG phantom margin using this setup a 775 nm pulsed DeltaDiode laser operating at an 80 MHz repetition rate was employed for excitation. An 801 nm dichroic mirror (Edmund Optics) with a reflection range of 450–790 nm and transmission window of 814–1100 nm was used to carry excitation light toward the sample, where an additional longpass filter transmitting above 800 nm (Thorlabs) was also utilized to minimize the collection of scattered light. Measurements were acquired at each position for 1 s, where the collected image size was 42.98 × 69.40 μm from an excitation spot of ~1 mm diameter delivered using an Olympus PLN 20× objective with a 0.4 NA and 1.1 mm FOV. The highly focused nature of the microscope optics and intrinsic resilience of APDs mean that unlike the LLG system the FLIM system can be operated in low level yet visually workable ambient light (in this case Skytile 3000 IP44 28W LED).

2.3. Materials and sample preparation

Silica alcogels were utilized in the phantom margin samples due to their reproducibility, negligible fluorescence, ease of production, high optical transmission and scattering and porous properties replicating features of human tissue. All

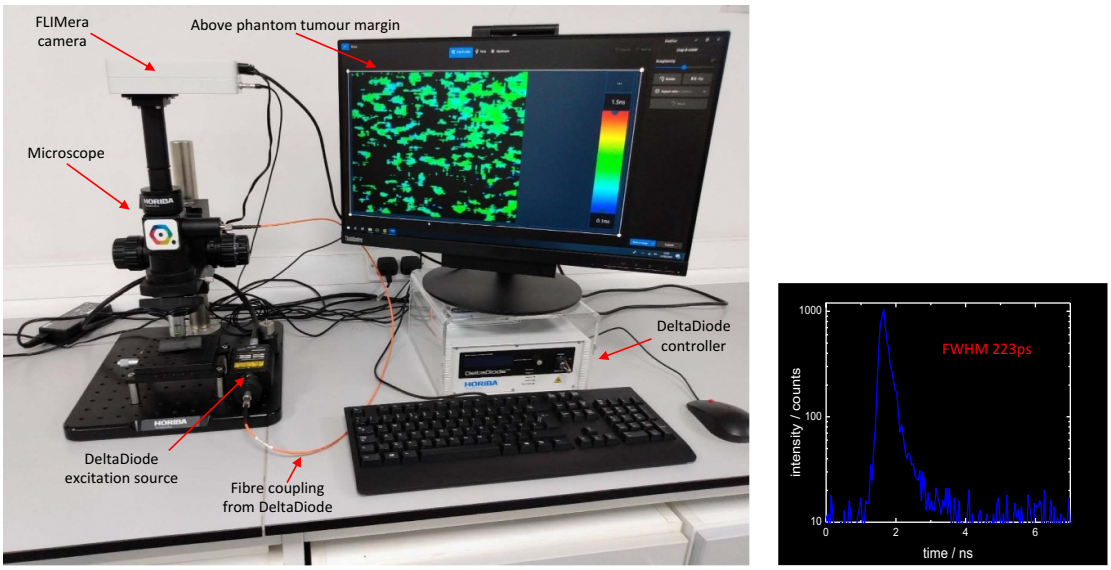

Figure 3. Photograph of the system setup incorporating the FLIMera fluorescence lifetime imaging camera and EzTime Image software for measurements of ICG phantom tumour margins, demonstrating the compact design of both the camera and full setup. The IRF of the system is also shown, which includes the laser optical pulse, SPAD response and TDC jitter.

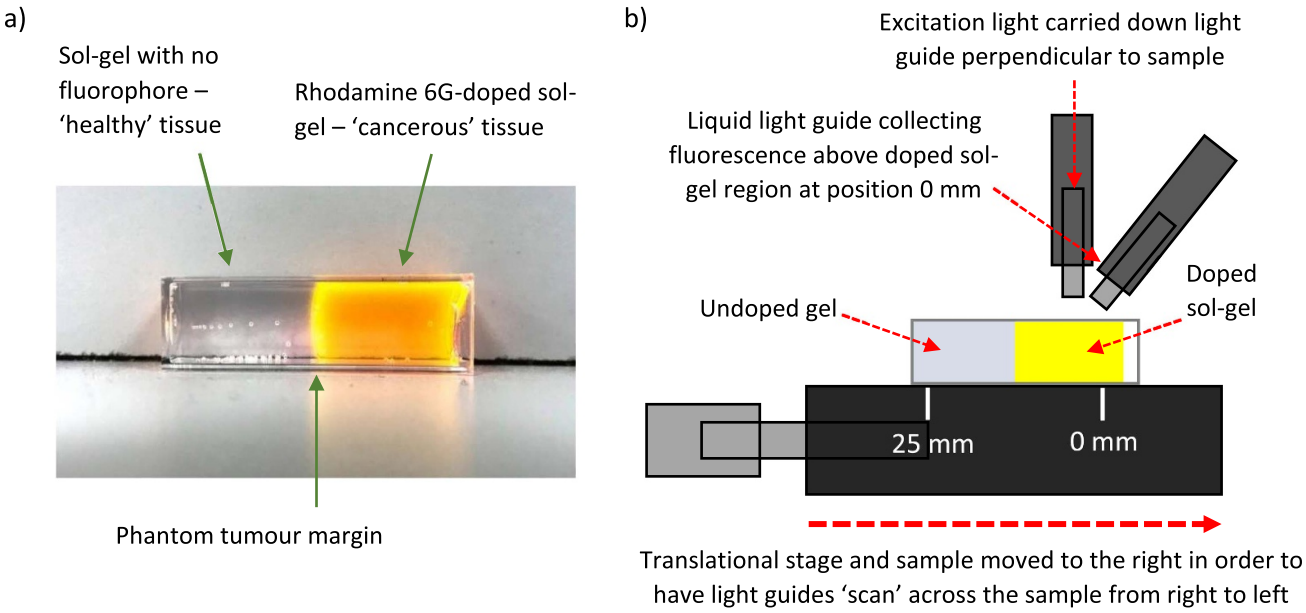

Figure 4. (a) Example of how a final phantom margin sample would appear, where highly concentrated R6G was used to clearly highlight the margin line in this sample contained in a cuvette of 10 × 10 × 45 mm internal dimensions. The sample setup on the translational stage for incremental measurements is shown in (b). The sample was initially positioned to have the light guide collecting fluorescence (light guide at 45° angle to sample) directly above the doped sol-gel edge at a 0 mm position. The light guides remained stationary as the stage was then moved in 1/2 or 1 mm increments as required towards the right, meaning the margin passed underneath the light guide collecting fluorescence at 15 mm as determined by visual inspection, and both light guides were above the sol-gel only region at the 25 mm position. Figure (b) not to scale.

chemicals were purchased from Sigma Aldrich. Silica alcogels were prepared using similar methods to those previously described [28], where initially 9 ml of TEOS was mixed with 3 ml of water and 0.2 ml of 0.01 M hydrochloric acid for ~2 h. Meanwhile, a stock solution of R6G was prepared by initially dissolving 1.44 mg of R6G in 30 ml of PBS, which was then further diluted by adding 1.8 ml of this stock to 28.2 ml of PBS, producing a final stock of 6 μM concentration. A stock of ICG was prepared in a similar way, where 1.16 mg of ICG was initially dissolved in 30 ml water which

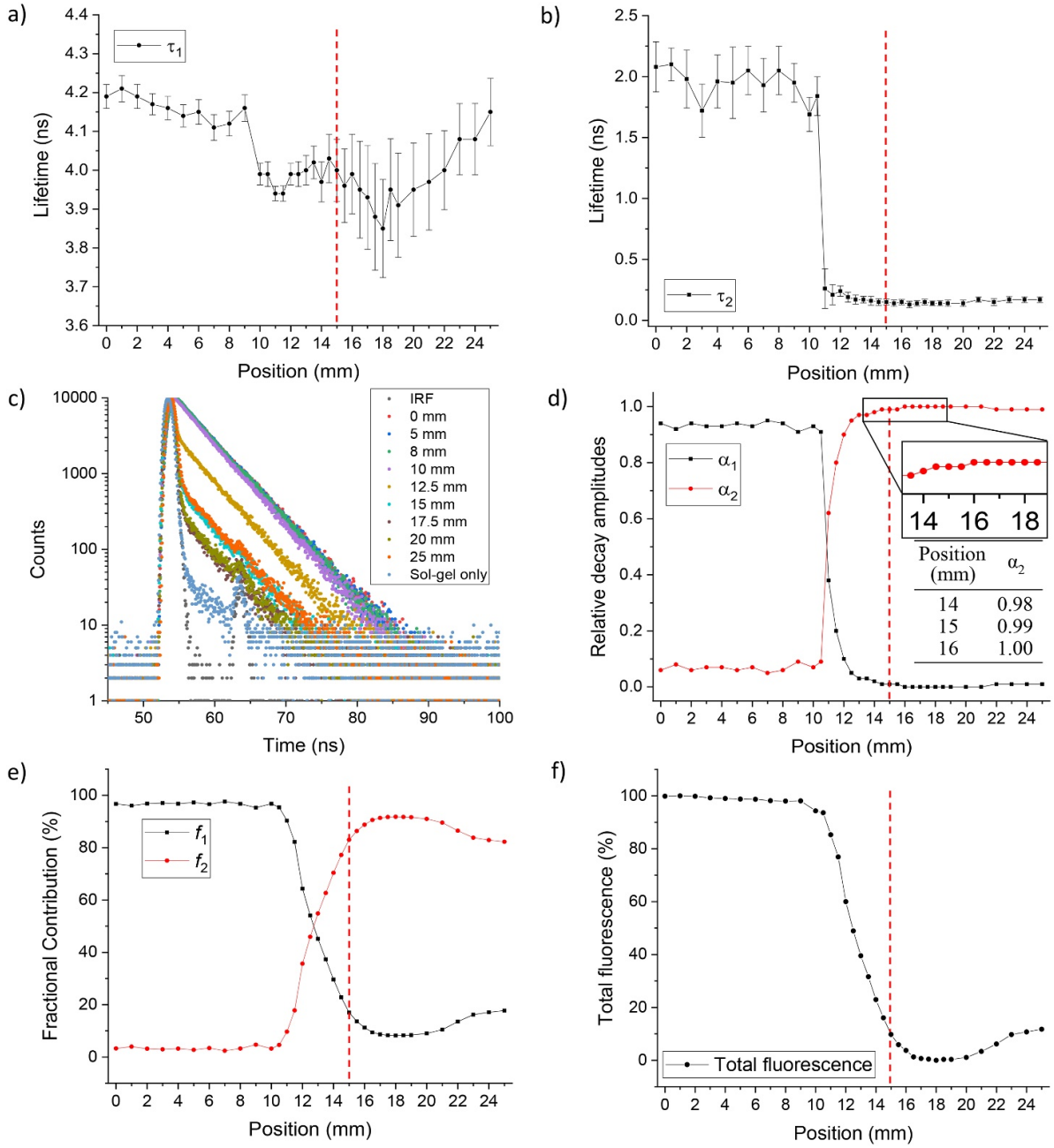

Figure 5. The change in (a) τ_1, (b) τ_2, (c) the fluorescence decays and instrumental response function (IRF) for the R6G-doped silica phantom, (d) the normalized pre-exponential values from equation (1), i.e. $\alpha_1 = B_1/(B_1 + B_2)$, $\alpha_2 = B_2/(B_1 + B_2)$ with expanded region and table values for α_2 across the phantom margin, (e) the fractional fluorescence intensity associated with each lifetime component at each position the sample was measured at i.e. $f_1 = B_1\tau_1/(B_1\tau_1 + B_2\tau_2)$ and $f_2 = B_2\tau_2/(B_1\tau_1 + B_2\tau_2)$ and (f) the total fluorescence intensity given by $B_1\tau_1 + B_2\tau_2$. The relative position of the centre of the fluorescence light guide is indicated on the x-axes with the margin position at 15 mm indicated by the red dashed line. The goodness of fit χ^2 values varied from 1.00 to 1.36 with an average of 1.16. Analysis with a three-exponential model produced no more precise trends, merely giving trade-offs between fitted parameters.

was further diluted by adding 1.2 ml of this stock to 28.8 ml PBS for a 2 μM stock. These concentrations were chosen in order to yield final samples that would have an absorbance of ~0.1, which is strong enough to generate a good fluorescence signal but not strong enough for dye-dye interactions to interfere [29].

The phantom margin was then prepared by first adding 1.2 ml of the TEOS solution and 1.2 ml of PBS only to a cuvette which was mixed and left to gel, where gelation occurred in ~30 min. This created the first 'layer' of gel to represent 'normal' human tissue. Once this had gelled, a further 1.2 ml of the TEOS solution and 1.2 ml of either the R6G or ICG stock as required was added. This was also mixed and left to gel, creating a second 'layer' to represent 'cancerous' tissue. The sample was contained in a standard polymethyl methacrylate UV cuvette of wall thickness 2 mm and internal

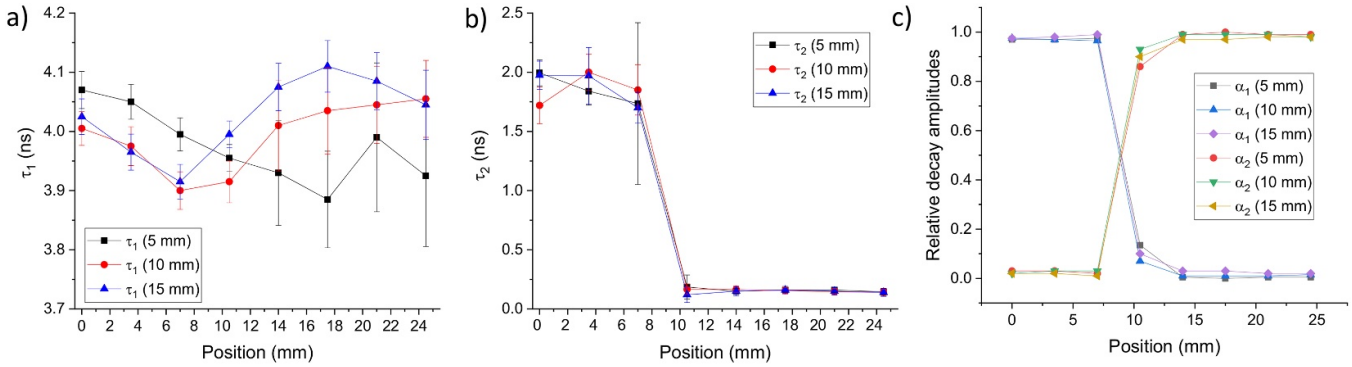

Figure 6. Comparison of (a) τ_1, (b) τ_2 and (c) their normalized pre-exponential values found at heights of 5 mm, 10 mm, and 15 mm above the R6G-doped silica phantom sample.

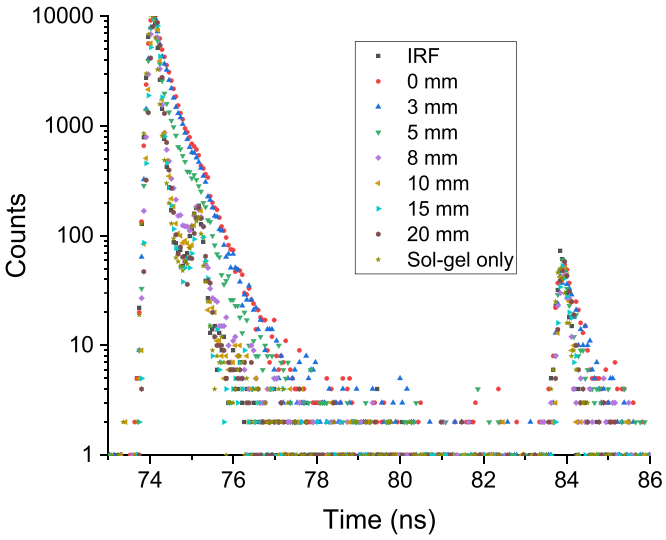

Figure 7. Fluorescence decays of the ICG phantom tumour margin sample at various positions. At 15 mm the light guide collecting fluorescence was directly above the margin point. The smaller peaks at ~10 ns after the main peaks are due to reflections from the end of the light guides.

dimensions 10 × 10 × 45 mm (Fisher Scientific). An illustration of how a final sample would look using a high concentration of R6G is shown in figure 4 as well as the setup of the sample on the translational stage in comparison to the light guide positions, where the light guides remain in a fixed position as the sample was moved towards the right using the stage.

3. Results and discussion

Measurements were taken of the R6G phantom margin sample at 1 mm increments until the light guides approached the margin, where measurements were then taken at $^1/_2$ mm increments to see how the fluorescence decay changed over such small distances as the margin was passed under the light guides. Figures 5(a) and (b) show the trend in best-fit fluorescence decay times obtained from non-linear least-squares fitting of the decay to the reconvolution of the IRF with equation (1) at various points across the margin for the raw decay data (figure 5(c)) including a sample containing the sol-gel only without R6G for comparison.

$$F(t) = A + B_1 \exp\left(-\frac{t}{\tau_1}\right) + B_2 \exp\left(-\frac{t}{\tau_2}\right). \qquad (1)$$

Here, A is the background noise, B is the pre-exponential function corresponding to the relative amount of each emitting species and τ_1 and τ_2 are the characteristic lifetimes associated with each fluorescent species/environment. The B values are given in the HORIBA IBH DAS6 analysis software and are weighted by their lifetime to give their fractional contributions $f_{1,2}$ to the total fluorescence as shown in figure 5(e).

The LLG collecting fluorescence was above the phantom margin at a position of 15 mm as determined from visual inspection. With respect to figure 5(c), which shows that at positions far away from the margin, when the light guides were above the R6G-doped sol-gel, the fluorescence decay strongly resembled that of R6G in water (table 1). However, although figure 5(a) indicates a lifetime value consistent with R6G for τ_1, and little changes are seen in its value regardless of position, the fact that the value of τ_1 is higher than 4 ns [30, 31] and gradually decreases towards the margin, suggests self-absorption facilitated by scattering from the silica matrix may be occurring. The analysis finding a second weak component τ_2 ~ 2 ns before the margin further supports the presence of R6G having heterogeneous kinetics in silica [30, 31] as might be also expected in tissue.

The question arises as to how best to interpret the fluorescence decay information in terms of finding the margin. The objective therefore is to find the parameters which show the maximum rate of change with displacement and then, given the rapid speed of currently available fluorescence decay analysis, real-time informative information can then be conveyed to an automated surgical instrument or surgeon. Different parameters can be used for demarcation purposes. In addition to the characteristic lifetimes τ_1 and τ_2, we illustrate this for the normalized amplitudes B_1 and B_2 in terms of their relative values ($\alpha_{1,2}$), (figure 5(d)) and the fractional contribution to the total fluorescence intensity each

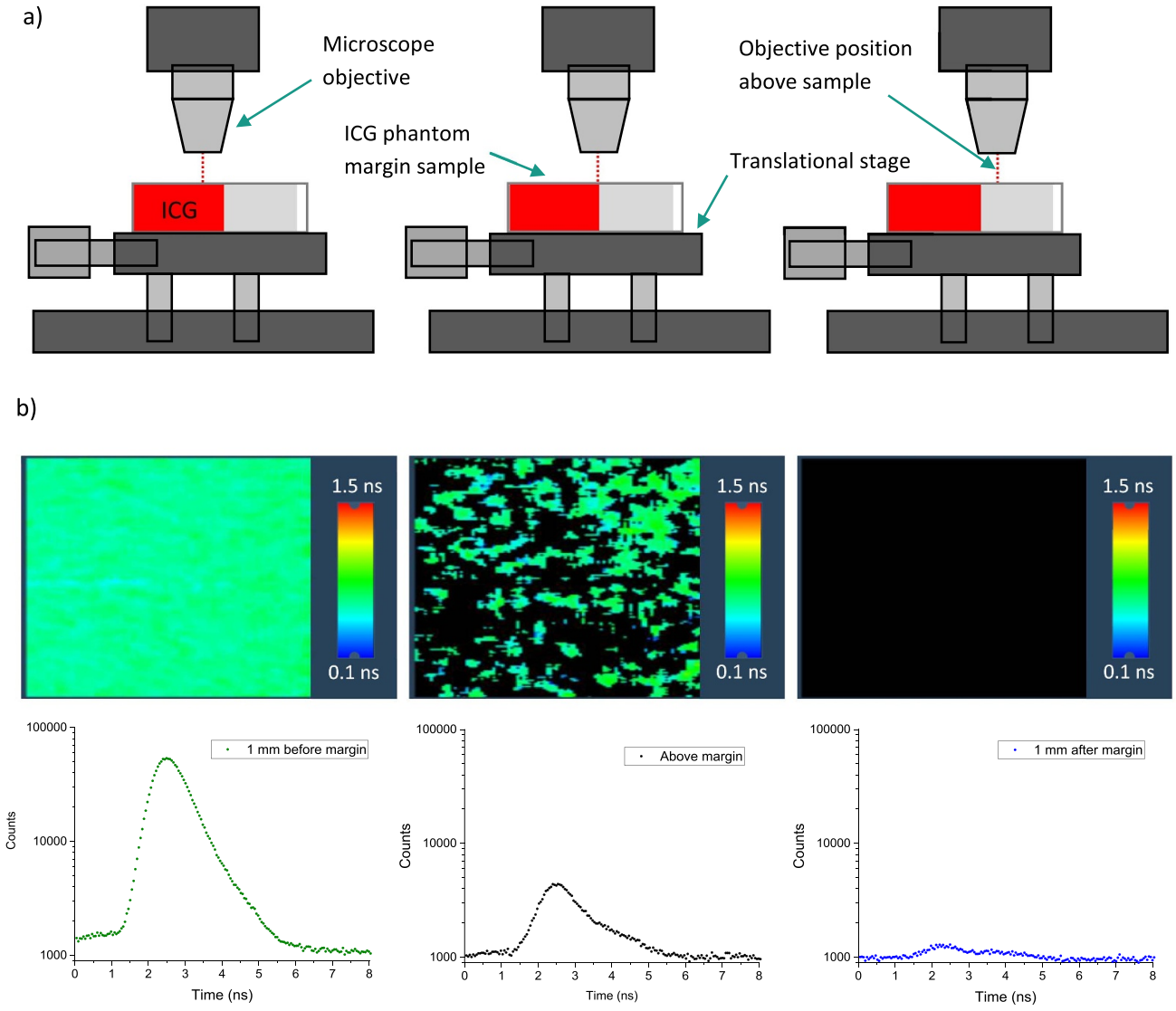

Figure 8. (a) Experimental setup for obtaining FLIM images and (b) the corresponding images and fluorescence decays, where the objective was 1 mm before the margin, above the margin and 1 mm after the margin. Distances in (a) have been exaggerated for clarity. Noise reduction has been applied at an intensity threshold of 30–500 photons to further remove noise. Image areas shown are 42.98 × 69.40 μm in size and the excitation spot was ~1 mm^2.

decay component provides ($f_{1,2}$), (figure 5(e)). The steady state equivalent using the total fluorescence intensity calculated from these measurements is also shown in figure 5(f), which closely resembles f_1 in figure 5(e) due to the τ_1 component being the biggest contributor to the total fluorescence intensity.

Figure 5(d) shows that as the light guides approached the margin at 15 mm the decay starts to fall more rapidly due to the scatter contribution from the sol-gel region now having a greater influence on the decay, where the relative contribution of R6G fluorescence first drops below 0.9 at the 11 mm position and τ_2 is ~0.1 ns. Similar values of ~0.15 ns are seen for τ_2 in samples of the sol-gel alone. While there is good agreement in the τ_2 values of the phantom margin sample and a sol-gel only sample, the fractional contributions $f_{1,2}$ and relative decay amplitudes $\alpha_{1,2}$ are better indicators of when the light guides have fully traversed the margin, as the value of τ_2 is in good agreement with the sol-gel only sample from 13 mm onwards, which is before the margin position of 15 mm. Close to the margin, the $\alpha_{1,2}$ values in figure 5(d) show the highest rate of change as well as the greatest consistency after the margin is traversed out of all the parameter combinations investigated. α_2 reaches 1.00 at 16 mm, which is the same value obtained for α_2 in the sol-gel only. This therefore provides an example of a figure of merit that could be used, where the sol-gel region can be confidently identified 1 mm after the margin position based on the obtained relative decay amplitude value $\alpha_2 = 1.00$ from this point onwards.

Measurements of the R6G phantom were also taken with the LLG system at 5 mm, 10 mm and 15 mm heights above the sample and at various points across the sample to see how

the values were affected. Figure 6 shows a comparison of the lifetime components and relative amplitudes of each decay component at each height at the different positions measurements were taken at. The values obtained for τ_1, τ_2, α_1 and α_2 were found to be consistent regardless of the height from the samples the measurements are performed at, demonstrating that the light guides do not need to be at a specific height from a sample in order to accurately measure either the lifetime values or the relative decay amplitudes. This is useful for practical implementation.

ICG was also studied in a phantom margin environment using the LLG setup. ICG was selected due to its widespread use by virtue of being the only FDA approved dye with excitation and fluorescence wavelengths compatible with the near infra-red transmission of tissue [20]. A selection of the fluorescence decays obtained at different positions are shown in figure 7. The decays shown in figure 7 highlight how fast the fluorescence lifetime of ICG is, where an average lifetime of 0.32 ns was found for the decay obtained at the 0 mm position. The data for such a short lifetime was extremely difficult to analyse as the decays were not much longer than the IRF, which defines the shortest possible decay that can be obtained from the system (here the FWHM of the IRF was 0.25 ns). The decays obtained also resembled the IRF from ~8 mm onwards when the light guides were still above the ICG-doped region and well before the margin at 15 mm. These results suggest the time resolution for the LLG system is not precise enough for measuring the decay of such short-lived species and as such is not workable in tumour margin estimation with ICG and similar dyes with such short lifetimes.

Consequently FLIM measurements were also made of ICG in a phantom margin using the prototype HORIBA IBH FLIMera TCSPC camera system, described previously [22], to assess whether this system would be more suitable for determining the margin position using ICG. Figure 8 shows the FLIM images obtained before, on, and after the margin along with the corresponding fluorescence decays for each image. The images before and after the margin are at the positions closest to the margin where the image and decays entirely resembled the ICG-doped region and sol-gel only region respectively. A two-exponential fit of the decay of ICG 1 mm before the margin, as shown in figure 8 and analysed with equation (1) was used, giving an average lifetime of 0.44 ns. This appears to be in good agreement with the corresponding FLIM image when compared to the scale. Noise reduction (median filtering) has been applied to the images and decays at 30–500 counts. Increasing the lower limit removes pixels with a low number of photons, which can therefore influence the obtained FLIM image and not accurately represent the sample. Figure 8 also shows that when the objective is directly above the margin, ICG fluorescence is still detected due to the finite width of the margin, but is significantly reduced in comparison to what is observed 1 mm before the margin. Similarly, just 1 mm after the margin there is minimal fluorescence detected from ICG, where the image and decay mainly correspond to out of focus emission. These results demonstrate the improved sensitivity of the FLIM system in comparison to the conventional lifetime spectroscopy provided by the LLG system setup for measuring the change in the fluorescence decay of ICG in the phantom margin environment. ICG was the dominant component in the FLIM measurements right up to the margin position whereas the sol-gel component was dominant in the LLG measurements 7 mm before the margin was even reached. A video of the scan across the phantom margin from which figure 8(b) is taken is shown in the Supporting Information (available online at stacks.iop.org/MST/31/125701/mmedia)

4. Conclusions

Silica alcogels have been utilized for creating phantom tumour margins to test the ability of a LLG and translational stage-based fluorescence lifetime system as well as a SPAD FLIM array system for determining the margin position. Despite the 3 mm diameter light guide giving ~7 mm excitation diameter it was found using R6G as the fluorophore in the doped sol-gel region that the relative decay amplitudes from the fluorescence decays obtained 1 mm after the margin resembled that of sol-gel only when measured with the LLG-based system, suggesting a satisfactory and workable level of surgical precision. While acceptable surgical margins can vary depending on factors such as the type of cancer and even the country where the surgery takes place, values as small as 1 mm have been reported as the minimal acceptable clearance distance for certain cancers [32, 33]. Fluorescence lifetime spectroscopy has been demonstrated here to be capable of such precision from measurements that take <2 min to conduct. This setup could be potentially developed for determining surgical margins or for the calibration of future surgical instruments based on fluorescence lifetimes but would benefit from further work such as studies in more complex tissue phantom environments (e.g. pigmented) and real tissue samples.

In addition to R6G, ICG was also studied in the phantom margin environment. It was found that the LLG-based system was not suitable for determining the margin position as precisely with ICG compared to R6G, as the system was unable to detect any longer lived ICG fluorescence, but only the temporal signature akin to the IRF due to scatter from the sol-gel from 7 mm before the margin. FLIM measurements provided a much better estimation of the margin position for ICG, where the image and corresponding fluorescence decays obtained just 1 mm after the margin represented the sol-gel region only. These measurements demonstrate the potential capabilities of such a system in margin estimation, where an ability to obtain images in almost real-time that show clear differences between a cancerous tissue region and healthy tissue region to 1 mm precision could provide a convenient and relatively easy-to-use method for determining surgical margins intraoperatively.

Charge coupled devices (CCDs) are universally the detector of choice at present for developments with steady-state fluorescence guided surgery [20]. Imaged intensified CCDs with higher sensitivity and gated variants for FLIM are also becoming more widely used [34]. The potential of multiplexing

TCSPC data in FLIM imaging was first demonstrated using multi-anode microchannel photomultipliers [35] but none of these photocathode-based systems offer the near infra-red sensitivity to match ICG as afforded by a SPAD camera. Not only do SPAD cameras bring to fluorescence-guided surgery the digital superiority of TCSPC but also this higher near infra-red spectral sensitivity of SPADs permits the use of lower pulse intensity/power (~10 pJ/mW average power) excitation, thus minimizing damage to cellular structures and the reporter dye. When combined with their intrinsic compactness, cellular level resolution to complement the macroscopic imaging that guides surgical incision and capability to operate in ambient light we believe SPAD cameras have much to offer the future of fluorescence-guided surgery.

Acknowledgments

We would like to thank the EPSRC and MRC Centre for the Doctoral Training in Optical Medical Imaging (OPTIMA) for a research studentship for HLS. We also wish to acknowledge the support of the QuantIC EPSRC Quantum Technologies Hub.

ORCID iDs

Hazel L Stewart https://orcid.org/0000-0002-1619-7202
Graham Hungerford https://orcid.org/0000-0002-9944-5688
David J S Birch https://orcid.org/0000-0001-6400-1270

References

[1] Observatory G C 2018 Cancer tomorrow: a tool that predicts the future cancer incidence and mortality burden worldwide from the current estimates in 2018 up until 2040 (available at: http://gco.iarc.fr/tomorrow/home (accessed 03 December 2019)
[2] CR UK 2019 Treat: develop new cancer treatments (available at: https://cancerresearchuk.org/funding-for-researchers/our-research-strategy/treat-develop-new-cancer-treatments) (accessed 03 December 2019)
[3] van Manen L, Handgraaf H J M, Diana M, Dijkstra J, Ishizawa T, Vahrmeijer A L and Mieog J S D 2018 A practical guide for the use of indocyanine green and methylene blue in fluorescence-guided abdominal surgery *J. Surg. Oncol.* **118** 283–300
[4] Harmsen S, Teraphongphom N, Tweedle M F, Basilion J P and Rosenthal E L 2017 Optical surgical navigation for precision in tumor resections *Mol. Imaging Biol.* **19** 357–62
[5] Chen Y, Xie W, Glaser A K, Reder N P, Mao C, Dintzis S M, Vaughan J C and Liu J T C 2019 Rapid pathology of lumpectomy margins with open-top light-sheet (OTLS) microscopy *Biomed. Opt. Express* **10** 1257
[6] Mondal S B, Gao S, Zhu N, Liang R, Gruev V and Achilefu S 2014 Real-time fluorescence image-guided oncologic surgery *Adv. Cancer Res.* **124** 171–211
[7] Eggemann H, Ignatov T, Beni A, Costa S D, Ortmann O and Ignatov A 2013 Intraoperative ultrasound in the treatment of breast cancer *Geburtshilfe Frauenheilkd* **73** 1028–34
[8] Nguyen F T, Zysk A M, Chaney E J, Kotynek J G, Oliphant U J, Bellafiore F J, Rowland K M, Johnson P A and Boppart S A 2009 Intraoperative evaluation of breast tumor margins with optical coherence tomography *Cancer Res.* **69** 8790–6
[9] Dumitru D, Douek M and Benson J R 2018 Novel techniques for intraoperative assessment of margin involvement *E-cancer Med. Sci.* **12** 795
[10] DeLong J, Hoffman R M and Bouvet M 2016 Current status and future perspectives of fluorescence-guided surgery for cancer *Expert Rev. Anticancer Ther.* **16** 71–81
[11] Wang M, Tang F, Pan X, Yao L, Wang X, Jing Y, Ma J, Wang G and Mi L 2017 Rapid diagnosis and intraoperative margin assessment of human lung cancer with fluorescence lifetime imaging microscopy *BBA Clin.* **8** 7–13
[12] Wallrabe H, Svindrych Z, Alam S R, Siller K H, Wang T, Kashatus D, Hu S and Periasamy A 2018 Segmented cell analyses to measure redox states of autofluorescent NAD(P)H, FAD & Trp in cancer cells by FLIM *Sci. Rep.* **8** 1–11
[13] Chacko J V and Eliceiri K W 2019 NAD(P)H fluorescence lifetime measurements in fixed biological tissues *Methods Appl. Fluoresc.* **7** 044005
[14] Gao R W *et al* 2018 Determination of tumour margins with surgical specimen mapping using near-infrared fluorescence *Cancer Res.* **78** 5144–54
[15] Van Terwisscha Scheltinga A G T, Van Dam G M, Nagengast W B, Ntziachristos V, Hollema H, Herek J L, Schröder C P, Kosterink J G W, Lub-de Hoog M N and De Vries E G E 2011 Intraoperative near-infrared fluorescence tumor imaging with vascular endothelial growth factor and human epidermal growth factor receptor 2 targeting antibodies *J. Nucl. Med.* **52** 1778–85
[16] 2019 PerkinElmer IVIS spectrum in vivo imaging system (available at: https://perkinelmer.com/uk/product/ivis-instrument-spectrum-120v-andor-c-124262) (accessed 03 December 2019)
[17] FLUOPTICS FLUOBEAM 2019 (available at: https://fluoptics.com/en/fluobeam/accessed) (accessed 03 December 2019)
[18] Bruschini C, Homulle H, Antolovic I M, Burri S and Charbon E 2019 Single-photon SPAD imagers in biophotonics: review and outlook *Light Sci. Appl.* **8** 1–28
[19] Homulle H A R *et al* 2016 Compact solid-state CMOS single-photon detector array for in vivo NIR fluorescence lifetime oncology measurements *Biomed. Opt. Express* **7** 1797
[20] DSouza A V, Lin H, Henderson E R, Samkoe K S and Pogue B W 2016 Review of fluorescence guided surgery systems : identification of key performance capabilities beyond indocyanine green imaging *J. Biomed. Opt.* **21** 080901-1-15
[21] Pogue B W, Rosenthal E L, Achilefu S and van Dam G M 2018 Perspective review of what is needed for molecular-specific fluorescence-guided surgery *J. Biomed. Opt.* **23** 100601-1-9
[22] Henderson R K, Johnston N, Della Rocca F M, Chen H, Li D D-U, Hungerford G, Hirsch R, McLoskey D, Yip P and Birch D J S 2019 A 192 × 128 time correlated SPADImage sensor in 40-nm CMOS technology *IEEE J. Solid-State Circuits* **54** 1907–16
[23] Birch D J S, Sanderson A, Holmes A S, McLoskey D and Imhof R E 1993 Miniaturized single-photon fluorometry *Meas. Sci. Technol.* **4** 797–9
[24] McGuinness C D, Sagoo K, McLoskey D and Birch D J S 2004 A new sub-nanosecond LED at 280 nm: application to protein fluorescence *Meas. Sci. Technol.* **15** L19-22

[25] Selanger K A, Falnes J and Sikkeland T 1977 Fluorescence lifetime studies of rhodamine 6G in methanol *J. Phys. Chem.* **81** 1960–3
[26] Geddes C D, Apperson K and Birch D J S 2000 New fluorescent quinolinium dyes - applications in nanometre particle sizing *Dyes Pigm.* **44** 69–74
[27] McLoskey D, Campbell D, Allison A and Hungerford G 2011 Fast time-correlated single-photon counting fluorescence lifetime acquisition using a 100 MHz semiconductor excitation source *Meas. Sci. Technol.* **22** 067001
[28] Hungerford G, Rei A, Ferreira M I C, Suhling K and Tregidgo C 2007 Diffusion in a sol-gel-derived medium with a view toward biosensor applications *J. Photochem. Photobiol. B: Biol.* **111** 3558–62
[29] Birch D J S, Yip P*et al* 2014 Nanometrology *Fluorescence Spectroscopy and Microscopy: Methods and Protocols* vol 1076, ed Y Engelborghs and A J W G Visser (Humana Press) pp 279–302 New York
[30] Black I, Birch D J S, Ward D and Leach M J 1997 The effect of ageing on the structure of wet sol-gel systems revealed by fluorescence resonance energy transfer *J. Fluoresc.* **7** 111–3
[31] Hungerford G, Suhling K and Ferreira J A 1999 Comparison of the fluorescence behaviour of rhodamine 6G in bulk and thin film tetraethylorthosilicate derived sol-gel matrices *J. Photochem. Photobiol. A: Chem.* **129** 71–80
[32] Endo M and Lin P P 2018 Surgical margins in the management of extremity soft tissue sarcoma *Chin. Clin. Oncol.* **7** 1–14
[33] Pilewskie M and Morrow M 2018 Margins in breast cancer: how much is enough? *Cancer* **124** 1335–41
[34] Sparks H *et al* 2017 Characterisation of new gated optical image intensifiers for fluorescence lifetime imaging *Rev. Sci. Instrum.* **88** 013707
[35] McLoskey D, Birch D J S, Sanderson A, Suhling K, Welch E and Hicks P J 1996 Multiplexed single-photon counting. I. a time-correlated fluorescence lifetime camera *Rev. Sci. Instrum.* **67** 2228–37